UC San Diego
Bioengineering
JACOBS SCHOOL OF ENGINEERING

University of California, San Diego

BENG 221

Mathematical Methods in Bioengineering

Mathematical Model for the Determination of Oxygen Spatial Maps in Microcirculatory Networks

---

Authors:
Anderson Scott, Niaz Nafea, Vivek Jani

January 22, 2018

Contents

1 Introduction

1.1 Background

Red Blood Cells (RBCs) are known to undergo time dependent biochemical and biophysical changes during storage, known as storage lesion [1, 2]. Biomolecules, namely 2,3 DPG, are depleted during storage, resulting in impaired oxygen delivery to tissues [3, 4]. Consequently, while arterial and venous saturation are maintained and improved after blood transfusion, oxygen delivery at the microcirculatory level is not [3, 5]. While many studies have demonstrated adverse effects due to blood transfusion, few have provided a reasonable mechanism by which storage lesion results in impaired oxygen delivery [1, 3]. Additionally, clinical metrics of blood oxygenation only consider systemic oxygen saturation and fail to account for changes in oxygen delivery at the microcirculatory level [4]. As such, current blood storage and transfusion protocols are inadequate in assessing tissue oxygenation.

Many studies have demonstrated both time-dependent and time-independent metrics to predict tissue oxygenation and the survival of transfused blood in clinical settings [1, 2]. However, these studies have failed to correlate these metrics with tissue oxygenation at the microcirculatory level [5, 6]. Clearly, there exists a need to develop mathematical models by which relationships between storage lesion and tissue oxygenation can be inferred. Classical microcirculatory oxygen delivery models, including the Krogh cylinder (Figure 1.1) have traditionally been used in research settings to quantify these changes [7, 8]. However, the Krogh cylinder model and updated iterations have been entirely theoretical and have failed to be implemented to support current research methods used to quantify changes in oxygen delivery [9, 10].

One method often used to quantify oxygen partial pressure (pO_2) in microcirculatory networks is phosphorescence quenching microscopy (PQM) [11]. An optical method, PQM uses a laser pulse to determine the amount of oxygen latent within the system. Phosphor dye (e.g. Palladium Polyporphyrin) is traditionally injected into animal models, and phosphor molecules are excited by means of a laser [12, 13]. Oxygen present within the volume can quench the laser excited phosphor molecules, and the rate of decay of phosphor excitation can be used to quantify oxygen partial pressure by means of the Stern-Volmer equation. However, measurement of oxygen by means of PQM depletes the oxygen concentration local to the volume of excitation. As such, while local regions of oxygen can be measured via this method, it is not possible to determine spatial oxygen maps accurately without additional mathematical methods.

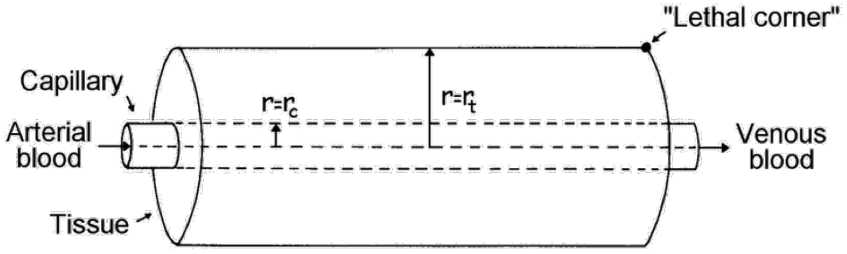

Figure 1.1: Classical Krogh Cylinder Model

Understanding the hemodynamics in the microcirculation from the perspectives of mass transport and fluid mechanics is advantageous. Mathematical quantification of tissue oxygen delivery from systemic parameters, like heart rate, blood pressure, arterial oxygen saturation, venous saturation, and blood viscosity, can provide evidence of adverse effects due to blood transfusion and be used to improve upon current blood storage and transfusion protocols. Additionally, these mathematical models can be used to more precisely treat pathologies associated with changes in blood oxygenation, including malaria, anemia, and polycythemia [14]. The objective of this mathematical model is to create a means to quantify changes in microcirculatory tissue oxygenation to better study effects of storage lesion on systemic tissue oxygenation and oxygen delivery. Utilizing data from animal models of the microcirculation, it is then possible to quantify tissue oxygenation from measured hemodynamics. In this way, quantitative studies of the effects of mechanical and biochemical storage lesion on tissue oxygenation and oxygen delivery can be implemented to better understand adverse effects of blood transfusion.

1.2 Problem Statement

Phosphorescence quenching microscopy is often used to measure local concentrations of oxygen partial pressure. However, the method itself is poor in resolution and unable to quantify oxygen spatial maps in animal models as oxygen is quenched during laser excitation of phosphor based dyes. As such, repeated measurements of oxygen utilizing PQM are unreliable at best in local regions. The objective of this model is to estimate oxygen partial pressure spatial maps from in vivo measurements to better understand spatial and temporal of oxygen maps in animal models. This model can then be used in animal models prior to better understand various pathophysiological phenomena associated with impaired oxygen delivery.

To simplify the situation, axial diffusion in the tissue is neglected. Rather, the problem is divided into infinitesimally thin blood vessel-tissue disks that are unable to interact with each other. A system of PDEs is solved for each disk, resulting in a discrete numerical solution of the entire problem.

2 Methods

2.1 Determination of pO_2

The method of phosphorescence quenching microscopy approximates O_2 partial pressures (i.e. pO_2) in the microcirculation. However, O_2 exists in two states in the blood vessel, freely dissolved in the plasma, or bound to hemoglobin (Hb). As first principles derive advection-convection diffusion relationships between flow, diffusivity, and oxygen concentration, it becomes necessary to determine the concentration of oxygen in a single arteriole given the pO_2. From fundamental chemical principles and Henry's Law, it is well known that the partial pressure of any gas is directly proportional to its concentration:

$$pO_2 = \alpha_{O_2} C_{O_2} \tag{1}$$

where α_{O_2} is defined as the Henry's Law Constant for oxygen. This relationship, however, neglects the oxygen bound to Hb. We define the Oxygen Saturation S_{O_2}, to be the proportion of oxygen

bound to Hb over the total Hb O_2 carrying capacity. Assuming a Hill Relationship between oxygen saturation and free oxygen, pO_2 is determined as follows:

$$pO_2 = \alpha_{O_2}(S_{O_2}[Hb]C_{O_2}) \tag{2}$$

where $[Hb]$ is the concentration of Hemoglobin, traditionally experimentally determined by spectroscopy, and S_{O_2} is the oxygen saturation, which is assumed to be the systemic oxygen saturation in this model. Therefore, utilizing systemic parameters and fundamental chemical principles, it is possible to determine oxygen concentration from oxygen partial pressure.

2.2 Steady State Solution

The diffusion convection equation is defined as follows:

$$\frac{\partial c}{\partial t} = \nabla \cdot (D\nabla c) - \nabla \cdot (\vec{v}c) + R \tag{3}$$

Inside the blood vessel, we make the following assumptions:

1. Steady State: $\frac{\partial c}{\partial t} = 0$
2. Neglect diffusion: $\nabla \cdot (\vec{v}c) >> \nabla \cdot (D\nabla c)$
3. $R = k_{leak}c$
4. Pipe Flow: $\vec{v} = (0, 0, v_z(r))$

We can therefore simplify the problem as follows:

$$-v_z \frac{\partial c}{\partial z} = k_{leak}c \tag{4}$$

with the following boundary conditions:

$$\begin{aligned} c(0) &= O_2^{IN} \\ c(L) &= O_2^{OUT} \end{aligned} \tag{5}$$

where L is the length of the blood vessel.

Utilizing the first boundary condition, $c(0) = O_2^{IN}$, the solution to the differential equation is as follows:

$$c_{in}(z) = O_2^{IN} exp\bigg(- \frac{k}{v_z} z \bigg) \tag{6}$$

Solving for k_{leak} utilizing the boundary condition $c(L) = O_2^{OUT}$, we find:

$$O_2^{OUT} = O_2^{IN} exp\bigg(- \frac{k_{leak}}{v_z} L \bigg) \tag{7}$$

$$k_{leak} = \frac{v_z}{L} ln \bigg| \frac{O_2^{IN}}{O_2^{OUT}} \bigg| \tag{8}$$

Substituting into equation (6), we find:

$$c_{in}(z) = O_2^{IN} \bigg(\frac{O_2^{OUT}}{O_2^{IN}} \bigg)^{z/L} \tag{9}$$

To determine the oxygen profile in the tissue, we simplify the problem into a series of N radial diffusion problems, each with initial condition $r(0) = \Phi c_{in}(x)$ for all $x/leqL$, where Φ is the Partition Coefficient. In this schema, we consider the following assumptions:

1. Steady State: $\frac{\partial c}{\partial t} = 0$
2. Neglect Convection: $\nabla \cdot (\vec{v}c) << \nabla \cdot (D \nabla c)$
3. Neglect Axial Diffusion: $\frac{\partial c}{\partial z} = 0$

In this schema, we obtain the following equation:

$$D \frac{\partial^2 c}{\partial r^2} + \frac{D}{r} \frac{\partial c}{\partial r} + k_{cons} c = 0 \tag{10}$$

where D is the diffusivity of oxygen in the tissue and k_{cons} is the consumption rate of oxygen by the tissue. We then define the following boundary conditions:

$$c_{out}(R) = \Phi c_{in}(x) \tag{11}$$

$$C_{out}(\infty) = 0 \tag{12}$$

where R is the radius of the vessel.

We then rewrite equation (10) as follows:

$$r^2\frac{\partial^2 c}{\partial r^2} + r\frac{\partial c}{\partial r} + \left(r^2\sqrt{\left|\frac{k_{cons}}{D}\right|^2} - 0^2\right)c = 0 \tag{13}$$

Notice that because $k_{cons} < 0$ and $D > 0$, the solution is the Modified Bessel Equation of order $n = 0$. As such, the solution must have the following form:

$$c_{out}(r) = AI_0\left(\sqrt{-\frac{k_{cons}}{D}}r\right) + BK_0\left(\sqrt{-\frac{k_{cons}}{D}}r\right) \tag{14}$$

Assuming that $|c(r)| < \infty$, we can claim that $A = 0$. Solving for B utilizing the boundary conditions yields:

$$B = \frac{\Phi c_{in}(x)}{K_0\left(\sqrt{-\frac{k_{cons}}{D}}R\right)} \tag{15}$$

Therefore,

$$c_{out}(r,x) = \frac{\Phi c_{in}(x)}{K_0\left(\sqrt{-\frac{k_{cons}}{D}}R\right)}K_0\left(\sqrt{-\frac{k_{cons}}{D}}r\right) \tag{16}$$

To determine k_{cons}, we utilize the principles of mass balance. Assuming that all oxygen entering the tissue is consumed, we can determine k_{cons} as follows:

$$k_{cons} = \Phi k_{leak} \tag{17}$$

2.3 Non-Steady State Solution: Inside the Blood Vessel

The diffusion convection equation is defined as follows:

$$\frac{\partial c}{\partial t} = \nabla\cdot(D\nabla c) - \nabla\cdot(\vec{v}c) + R \tag{18}$$

We make the following assumptions:

1. Neglect diffusion: $\nabla \cdot (\vec{v}c) >> \nabla \cdot (D \nabla c)$
2. $R = k_{leak} c$
3. Pipe Flow: $\vec{v} = (0, 0, v_z)$
4. Assume that the input and output oxygen profiles sinusoidally with frequency equivalent to the heart rate.

We are therefore solving the problem:

$$\frac{\partial c}{\partial t} + v_z \frac{\partial c}{\partial z} = k_{leak} c \tag{19}$$

Boundary Conditions:

$$c(0,t) = sin\left(\frac{\pi HR}{30} t\right) + O_2^{IN} = f(t) \tag{20}$$

$$c(L,t) = sin\left(\frac{\pi HR}{30} t\right) + O_2^{OUT} = g(t) \tag{21}$$

Utilizing the method of characteristics, we parametrize a surface $q(\gamma, s)$ to define the solution $c(z,t)$.

$$\frac{\partial t}{\partial s}(\gamma, s) = 1 \tag{22}$$

$$\frac{\partial z}{\partial s}(\gamma, s) = v_z \tag{23}$$

$$\frac{\partial q}{\partial s}(\gamma, s) = k_{leak} q \tag{24}$$

BC:

$$t(\gamma, 0) = \gamma \tag{25}$$

$$z(\gamma, 0) = v_z \tag{26}$$

$$q(\gamma, 0) = k_{leak} q \tag{27}$$

Solutions:

$$t(\gamma, s) = \gamma + s \tag{28}$$

$$z(\gamma, s) = v_z s \tag{29}$$

$$q(\gamma, s) = c(\gamma) e^{k_{leak} s} \tag{30}$$

Solving for $\gamma(z,t)$ and $s(z,t)$:

$$s = \frac{z}{v_z} \tag{31}$$

$$\gamma = t - \frac{z}{v_z} \tag{32}$$

Solution is therefore:

$$c(z,t) = f\left(t - \frac{z}{v_z}\right) \tag{33}$$

Solve for k_{leak} utilizing the other BC:

$$k_{leak} = \frac{v_z}{L} ln\left|\frac{f(t - L/v_z)}{g(t)}\right| \tag{34}$$

Substituting for k_{leak}

$$c(z,t) = f(t - z/v)\left(\frac{g(t)}{f(t - L/v)}\right)^{z/L} \tag{35}$$

2.4 Non-Steady State Solution: Outside the Blood Vessel

The problem in the radial direction in the tissue is defined as follows:

$$\frac{\partial c}{\partial r} = D\frac{\partial^2 c}{\partial r^2} + \frac{D}{r}\frac{\partial c}{\partial r} + kc \tag{36}$$

where $k = \Phi k_{leak}(t = 0)$, as determined in the axial solution above.

Boundary Conditions:

$$c(R, t) = \Phi c_{in}(z, t) = h_l(t) \tag{37}$$

$$c(\infty, 0) = 0 \tag{38}$$

where $l \in \mathbb{Z}$. In this case, we discretize the problem in z. Therefore, we assume a single time dependent distribution for each z_l, $h_l(t)$.

Initial Condition

$$c(r, 0) = \Phi c_{in}(z, 0)10^{(R-r)/4R} = f_l(r) \tag{39}$$

where $l \in \mathbb{Z}$ for each z_l.

Step 1: Solve the Steady State Problem with BCs shown above. The solution to this problem is $b(r, t)$.

$$D\frac{\partial^2 b}{\partial r^2} + \frac{D}{r}\frac{\partial b}{\partial r} + kb = 0 \tag{40}$$

We know this solution:

$$b(r, t) = A(t)K_0\left(\sqrt{-\frac{k}{D}}r\right) \tag{41}$$

Substituting the BC yields:

$$A(t) = \frac{h_l(t)}{K_0\left(\sqrt{-\frac{k}{D}}R\right)} \tag{42}$$

The solution is therefore,

$$b(r,t) = \frac{h_l(t)}{K_0\left(\sqrt{-\frac{k}{D}}R\right)} K_0\left(\sqrt{-\frac{k}{D}}r\right) \tag{43}$$

Step 2: Define $v(r,t) = c(r,t) - b(r,t)$ and determine the problem for $v(r,t)$

$$\frac{\partial}{\partial t}(v+b) = D\frac{\partial^2}{\partial r^2}(v+b) + \frac{D}{r}\frac{\partial}{\partial r}(v+b) + k(v+b) \tag{44}$$

$$\frac{\partial v}{\partial t} = D\frac{\partial^2 v}{\partial r^2} + \frac{D}{r}\frac{\partial v}{\partial r} + kv - \frac{\partial b}{\partial t} \tag{45}$$

as

$$D\frac{\partial^2 b}{\partial r^2} + \frac{D}{r}\frac{\partial b}{\partial r} + kb = 0 \tag{46}$$

Initial Conditions:

$$v(r,0) = c(r,0) - b(r,0) = f_l(r) - b(r,0) = \bar{f}_l(r) \tag{47}$$

Boundary Conditions:

$$v(R,t) = c(R,t) - b(R,t) = h_l(t) - h_l(t) = 0 \tag{48}$$

$$v(\infty,0) = 0 \tag{49}$$

$$|v(r,t)| < \infty \tag{50}$$

Step 3: Extract the eigenfunctions and eigenvalues from the homogeneous equation for $v(r,t)$

$$\frac{\partial v}{\partial t} = D\frac{\partial^2 v}{\partial r^2} + \frac{D}{r}\frac{\partial v}{\partial r} + kv \tag{51}$$

$$v(r,t) = \phi(r)g(t) \tag{52}$$

$$\phi g' = D\phi'' g + \frac{D}{r}\phi' g + k\phi g \tag{53}$$

$$\frac{g'}{g} = \frac{D\phi'' + \frac{D}{r}\phi' + \phi}{\phi} = -\lambda \tag{54}$$

We now only need to solve the eigenfunction equation for ϕ:

$$D\phi'' + \frac{D}{r}\phi' + (k+\lambda)\phi = 0 \tag{55}$$

Case 1: $lambda < -k$

$$\phi(r) = AI_0\left(\sqrt{-\frac{k+\lambda}{D}}r\right) + BK_0\left(\sqrt{-\frac{k+\lambda}{D}}r\right) \tag{56}$$

Substituting in Boundary Conditions yields $A = B = 0$

Case 2: $\lambda = -k$

$$D\phi'' + \frac{D}{r}\phi' = 0 \tag{57}$$

$$\phi(r) = Aln|r| + B \tag{58}$$

Substituting in Boundary Conditions yields $A = B = 0$

Case 3: $\lambda > -k$

$$\phi(r) = AJ_0\left(\sqrt{\frac{k+\lambda}{D}}r\right) + BY_0\left(\sqrt{\frac{k+\lambda}{D}}r\right) \tag{59}$$

Substituting in Boundary Conditions yields $B = 0$. Therefore, the eigenfunctions take the form:

$$\phi_n(r) = A_n J_0\left(\sqrt{\frac{k+\lambda_n}{D}}r\right) \tag{60}$$

To find the eigenfunctions, substitute the other boundary condition:

$$A_n J_0\left(\sqrt{\frac{k+\lambda_n}{D}}R\right) = 0 \tag{61}$$

If $A_n = 0$, the solution is trivial. Therefore,

$$J_0\left(\sqrt{\frac{k+\lambda_n}{D}}R\right) = 0 \tag{62}$$

Define α_n be the roots of the Bessel function $J_0(x)$. Thus, the eigenvalues are numerically determined as:

$$\lambda_n = D\left(\frac{\alpha_n}{R}\right)^2 - k \tag{63}$$

In summary,

$$\phi_n(r) = A_n J_0\left(\sqrt{\frac{k+\lambda_n}{D}}r\right) \tag{64}$$

$$\lambda_n = D\left(\frac{\alpha_n}{R}\right)^2 - k \tag{65}$$

Step 5: Exploiting the Sturm-Liouville theorem, we write the solution $v(r,t)$ as an infinite series of eigenfuncitons:

$$v(r,t) = \sum_{n=0}^{\infty} a_n(t)\phi_n(r) \tag{66}$$

Substituting into the original differential equation yields:

$$\sum_{n=0}^{\infty} \frac{da_n}{dt}\phi_n(r) = \sum_{n=0}^{\infty} \left(D\phi'' + \frac{D}{r}\phi' + k\phi \right) a_n(t) - \frac{\partial b}{\partial t} \tag{67}$$

As $\phi_n(r) = -\lambda_n \phi_n(r)$

$$\sum_{n=0}^{\infty} \left(\frac{da_n}{dt} + \lambda_n a_n(t) \right) \phi_n(r) = -\frac{\partial b}{\partial t} \tag{68}$$

We do the same thing for $-\frac{\partial b}{\partial t}$:

$$\sum_{n=0}^{\infty} \left(\frac{da_n}{dt} + \lambda_n a_n(t) \right) \phi_n(r) = \sum_{n=0}^{\infty} c_n(t)\phi_n(r) \tag{69}$$

To solve for $b_n(t)$, we exploit the orthogonality of the Bessel Functions:

$$\int_0^{\infty} \phi_n(r)\phi_m(r) r \sqrt{-\frac{k}{D}} dr = 0, m \neq n \tag{70}$$

Therefore,

$$c_n(t) = -\frac{\partial b}{\partial t} \frac{\int_R^{\infty} \phi_n(r) r dr}{\int_R^{\infty} \phi_n^2(r) r dr} \tag{71}$$

To find $a_n(t)$, we solve the following differential equation:

$$\frac{da_n}{dt} + \lambda_n a_n(t) = c_n(t) \tag{72}$$

as both λ_n and $c_n(t)$ are known, it is then possible to find $a_n(t)$, as shown in the Numerical Methods section.

To find the initial condition, we perform again exploit the orthogonality of eigenfunctions:

$$a_n(0) = \frac{\int_R^\infty \bar{f}(r)\phi_n(r)rdr}{\int_R^\infty \phi_n^2(r)rdr} \tag{73}$$

2.5 Numerical Methods

Determination of the Eigenvalues λ_n. To determine the eigenvalues, it was necessary to find the roots α_n of the Bessel Function of the First Kind $J_0(r)$. To do so, Halley's method was employed. Let $J_0'(r)$ be the numerically determined central finite difference of the Bessel Function of the First Kind and $J_0''(r)$ be the numerically determined central difference as shown:

$$J_0'(r) = \frac{dJ_0(r)}{dr} = \frac{J_0(r+\Delta r) - J_0(r-\Delta r)}{2\Delta r} \tag{74}$$

$$J_0''(r) = \frac{J_0(r+\Delta r) - 2J_0(r) + J_0(r-\Delta r)}{\Delta r^2} \tag{75}$$

Utilizing (74) and (75) , the roots, α_n were iteratively determined as follows:

$$\alpha_{n+1} = \alpha_n - \frac{2J_0(\alpha_n)J_0'(\alpha_n)}{2[J_0(\alpha_n)]^2 - J_0(\alpha_n)J_0''(\alpha_n)} \tag{76}$$

for a sufficiently close guess α_n. Depending on the value of n, the iteration in (76) is repeated to find a sufficient number of roots.

Determination of $a_n(t)$. The coefficients of the solution $a_n(t)$ were determined utilizing Euler's method with a sufficiently small step size Δt to ensure convergence. From (72), we find that

$$a_n(t+\Delta t) = a_n(t) - \left(\lambda_n a_n(t) + \frac{\partial b}{\partial t}\right)\Delta t \tag{77}$$

Determination of $a_n(0)$ and $c_n(t)$. To determine $a_n(0)$ and $c_n(t)$ from (73) and (71), respectively, the trapezoidal method of numerical integration was employed. As such, the integrals in (73) and (71) were evaluated as follows. Let $y(t)$ be some function that needs to be integrated. As such:

$$\int_{y_0}^{y_n} y(t)dt \approx \sum_{k=1}^{N} \frac{y_{k+1} - y_k}{2} \Delta t \tag{78}$$

3 Results

All solutions to the found equations were graphed in Matlab_R2015 (Mathworks, 2015). Plot generation code is found in the appendix.

3.1 Steady State Solution

Axial Distribution of Oxygen Inside the Blood Vessel: To best understand the non-linear time dynamics of the model, the steady state solution was first analyzed. The oxygen saturation profile inside the blood vessel $C_{in}(z)$ is represented in Figure 3.1. This profile demonstrates the relevance of length scale when analyzing the oxygen distribution in the model along z. At small length scales (i.e. on the scale of microcirculatory vessels), we observe a pseudo-linear dependence of oxygen concentration on z. However, first order leak kinetics impose an exponential dependence on z, as demonstrated in Figure 3.1. Additionally, Figure 3.1 demonstrates a major limitation of the model as O_2 concentration does not vary with radius, as assumed. However, in the context of this model, the distribution of red cells in microvessels validates this assumption.

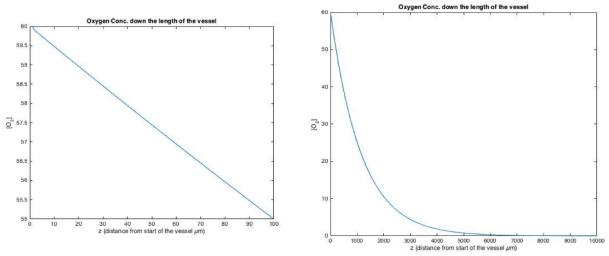

Figure 3.1: Comparing length scales for the axial steady state model

Radial Distribution of Oxygen in the Tissue: By conservation of mass, the solution of oxygen inside the blood vessel was used to determine the boundary condition of $[O_2]$ in the surrounding tissue. As demonstrated in the Methods, the spatial dynamics of this oxygen distribution can be approximated using a Modified Bessel Function of the Second Kind. This graphical solution can be seen in Figure 3.2 below. An important aspect of this model is the propagation of the axial concentration gradient away from the center of the blood vessel, seen at a distance of 80 μm from the vessel. Additionally, it is important to note the limitation of this graphical representation. A more accurate representation of this model would show the oxygen profile at any distance and angle from the plane that is represented here.

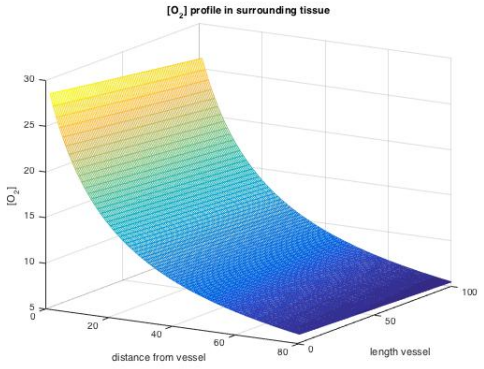

Figure 3.2: Steady State Oxygen profile in tissue surrounding the blood vessel

A complete representation of the model involves a numerical combination of the models solved both inside and outside the blood vessel, as demonstrated in Figure 3.3. Data from inside the blood vessel and the surrounding tissue were combined to form a clear plane. This plane includes the vessel and tissue on either side. To do this, the data matrix derived for the tissue was rotated 180 degrees, then the rotated tissue matrix, vessel data matrix, and non-rotated tissue matrix were combined to form a this final matrix. Graphically, this is seen below in Figure 3.3.

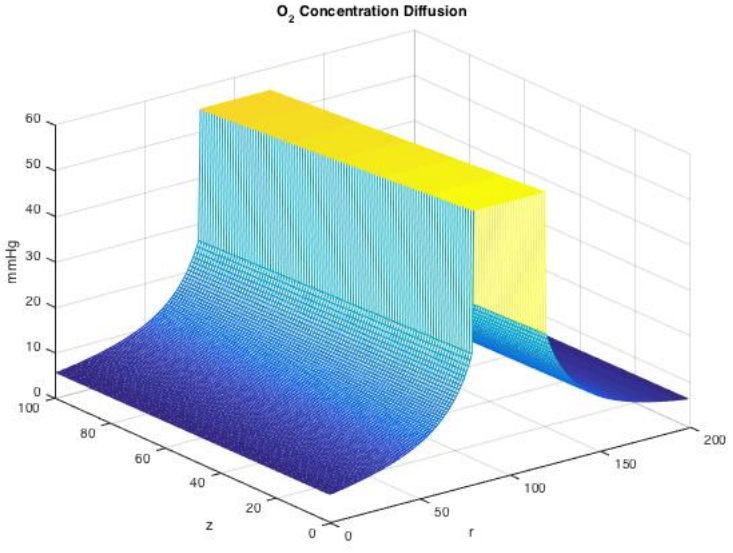

Figure 3.3: Steady State Solution

Determination of Oxygen Spatial Map in a Microcirculatory Network This simplified limitation was used to verify some of the properties seen in biological systems and in the context of microcirculatory networks. Namely, we wanted to utilize this steady state model to see the effects of having two vessels running parallel through a tissue. In order to implement this, we made the assumption

that this system was linear, and thus abides by superposition. In our model, superposition states that the effect on the oxygen concentration at some point in the tissue was the sum of all the effects of the surrounding vessels. As such, we can partially overlap two data matrices and then add the terms together. We also implemented a boundary condition that a single blood vessel can only supply oxygen to tissue and not to the interior of an adjacent blood vessel.

Computationally, a data matrix for the tissue was lengthened to give data up to 200μm away from the tissue. Then the data matrix was copied and rotated 180 degrees. Once an overlap length was determined, the two matrices were added together. Anything between the two local maxes, i.e. the spots where the tissue met the vessel on either data matrix, was kept, and the rest was removed (a digital xor operation). Finally, this new data matrix was combined with two vessel matrices and two tissue matrices to produce the final data matrix which was graphed using the mesh function on MATLAB. This graph can be seen below in Figure 3.4.

This figure verifies what is expected from the biology of the system. Oxygenation of the tissue between two adjacent blood vessels receives ample O_2 from either vessel. Once again, a limitation of this representation of the model is that it can only show the concentration across a plane that intersects the blood vessels. Blood vessels can only be added in planes in which they are viewed. Representing, for example, a third blood vessel underneath the two shown is not possible, and thus represents a limitation of the graphical representation of the model.

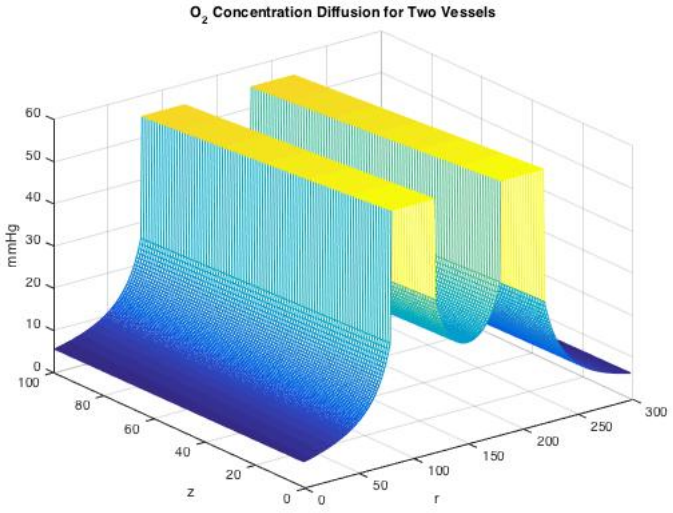

Figure 3.4: Steady State Microcirculatory Network Solution

3.2 Non-Steady State Solution

Single Vessel Non-Steady State Solution The complete non-steady state solution was plotted over time for a single blood vessel. Note that the frequency of oscillation is proportional to the heart rate of the animal model during data collection. Results are summarized in Figure 3.5. The non-steady state solution demonstrates a phase delay between propagation of the pressure wave and tissue

oxygenation, a phenomenon that demonstrates a degree of constant oxygenation independent of the heart rate. The complete non-steady solution was then recorded using QuickTime Player's screen recording option. The low resolution can be attributed to the computational intensity associated with determining the analytical solution.

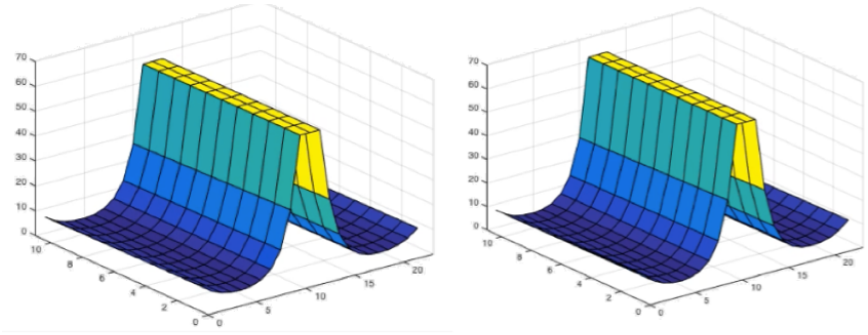

Figure 3.5: Non-Steady State Solution at Systole (left) and Diastole (right)

Non-Steady State Microcirculatory Network Results for a non-steady state microcirculatory network are summarized in Figure 3.6. As expected, tissue between two oxygen sources has higher oxygenation than any section of tissue with only one oxygen source. Once again, the crest peaks a little after 60 mmHg and minimizes at a little below 60 mmHg.

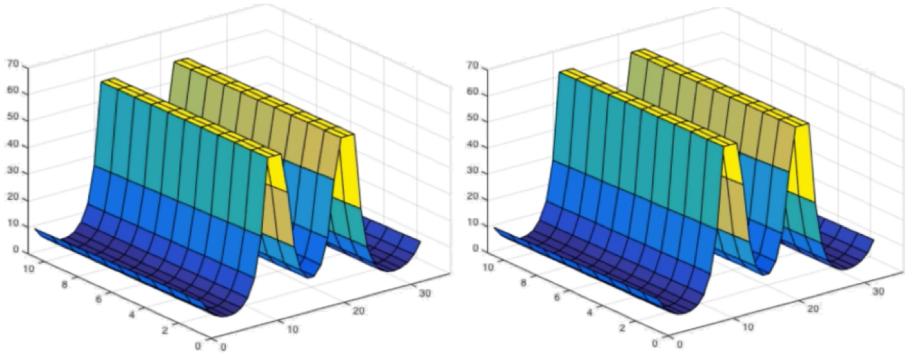

Figure 3.6: Non-Steady State Microcirculatory Network

Variation of the Tissue Oxygen Consumption Rate: The rate of tissue oxygen consumption, k, was modulated to investigate the effects of hypoxia and hyperoxia in the model developed by increasing and decreasing it by an order of magnitude. Results are summarized in Figures 3.8 and 3.7.

These results exemplify the sensitivity of the variables used, in addition to demonstrating the high degree of control that biological systems have with regard to oxygen consumption. For high oxygen consumption, which models hypoxic conditions, we see oxygen depletion of cells radially distant from the blood vessel edge. Likewise in hyperoxic conditions, modeled by low oxygen consumption, we notice accumulation of oxygen in the tissue, demonstrated by the flaring at either end of the blood vessel.

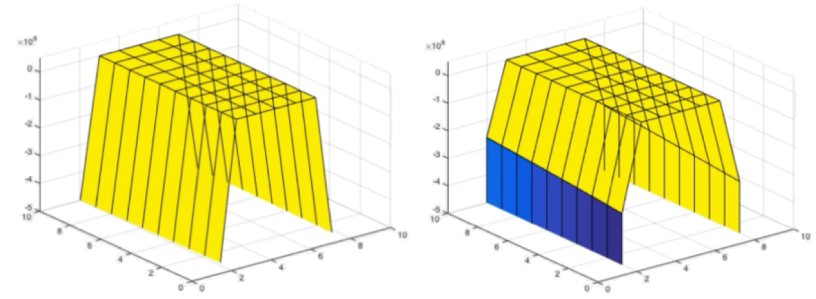

Figure 3.7: Modeling hypoxia: High Oxygen Consumption

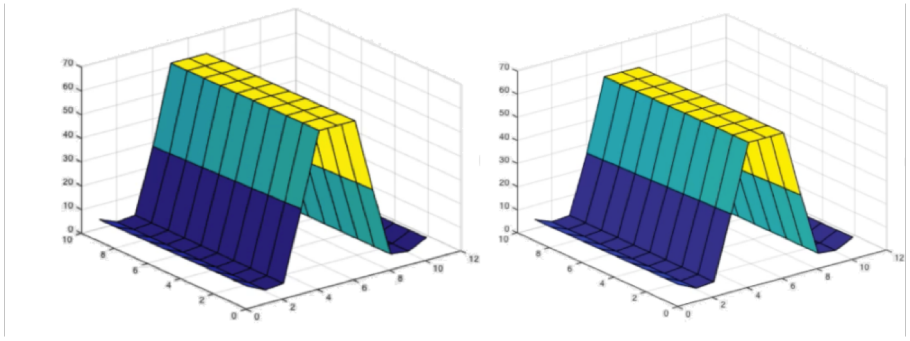

Figure 3.8: Modeling hyperoxia: Low Oxygen Consumption

4 Discussion

4.1 Steady State Solution

The principal findings of this model are that oxygen exponentially decays axially and radially following a Bessel Function of the First Kind. In addition, this model demonstrates that cells local to microcirculatory networks have the ability to finely tune their oxygen consumption, ensuring equal distribution of oxygen throughout the entire local tissue area. With respect to the steady state solution, this model demonstrates that oxygen decay is pseudo-linear, namely due to the small length scale. However, as length scale increases (i.e. for larger networks) the exponential decay of oxygen becomes more relevant (Figure 3.1). However, oxygen diffusion outside the blood vessel likely does not follow first order leak kinetics. As such, decay is likely to be slower than expected, causing changes which are likely to propagate radially down the tissue and change the oxygen spatial map.

As demonstrated in the steady state solution, the radial oxygen profile decays following a Modified Bessel Function of the Second Kind, due to the fact that the cells local to microvessels act as oxygen sinks. If for instance, a similar model was being used to model oxygen diffusion outside plant networks, the kinetics of the problem would vary drastically. The shape of the modified Bessel Function of the Second Kind mimics that of exponential decay and supports the idea that the problem is bounded, in addition to the fact that oxygen concentration decays exponentially as radius increases. Note that this is entirely an artifact of how the problem was defined. The

modified Bessel Function of the Second Kind is unbounded towards the limit as r approaches 0. For this reason, the boundary conditions were shifted, to ensure that a non-trivial solution exists.

A model of the oxygen map of a microcirculatory network was then created namely due to superposition. In addition to demonstrating the utility of having an effective geometry to oxygenate an entire tissue region, this model also demonstrates the utility of a countercurrent exchange system. As oxygen concentration is maximized between the two blood vessels, relative to either side of it, oxygen flux is also maximized. In this schema, if one of the blood vessels is an oxygen sink, a venuole, then flux is maximized in the region between the oxygen source, arteriole, and the venuole, demonstrating how countercurrent exchange systems provide a useful means of solute and heat transport. In addition, it is entirely possible to create a microcirculatory network with a unique geometry so as to induce a "hypoxic pocket" of tissue. With this schema in mind, it is then possible to calculate the optimal distance to maximize delivery of oxygen. More specifically, the distance at which a hypoxic pocket ceases to exist represents the maximum distance that any two blood vessels may be away from each other to maximize oxygen delivery to a given area of tissue.

One disadvantage to the steady state model, however, is the lack of a theoretical limit of oxygen transport, known as the Krogh radius. As later discussed, this phenomenon becomes more apparent in the non-steady state model.

4.2 Non-Steady State Solution

In addition to the points of analysis mentioned, the non-steady state model provides a means to analyze tissue oxygenation with regard to the systolic and diastolic phases of the cardiac cycle, or their equivalents at the microcirculatory level. In theory, tissue oxygenation should be minimized during diastole. However, this model demonstrates a phase difference between axial propagation of oxygen and the frequency of systole and diastole. This phase difference results in a constant level of tissue oxygenation independent of the heart rate, a phenomenon that is able to explain many mechanisms of vasocontrol at the microcirculatory level. For instance, vasomotion, the spontaneous change in vascular tone independent of heart rate, would result in local changes in the tissue oxygenation based on convective transport in a manner very similar to those due to the cardiac cycle. However, as demonstrated in this model, the phase delay between tissue oxygenation and other frequency dependent modulations of convective oxygen transport results in a relatively static level of oxygen radially downstream.

Another significant result of this model is the development of a theoretical limit of oxygen transport, known as the Krogh radius. After a certain point, approximately 100 μm away from the vessel edge, the solution becomes unstable and begins to flare. While this can be viewed as a limitation of the model, the point at which oxygen is minimized radially represents the theoretical limit of oxygen transport, a limit classically known as the Krogh radius. One major advantage of the non-steady state model is the appearance of this phenomenon. While the kinetics of oxygen transport, consumption, and diffusion remain relatively similar between models, this theoretical limit provides additional information of microcirculatory studies and can help provide a more complete mechanistic understanding of the effects of variations in the 3D spatial configuration of blood vessels on tissue oxygenation.

The model is also advantageous in its ability to qualitatively explain the deleterious effects of hypoxia and hyperoxia on tissue oxygenation at the microcirculatory level. Under both high and low oxygen consumption rates, hypoxia and hyperoxia respectively, we observed drastic changes in local oxygen concentrations. In the case of hypoxia, tissue radially farther from the blood vessel

edge is entirely depleted of oxygen. In hyperoxia, accumulation of oxygen includes reactive oxygen species, so it is equally harmful to cells.

One major disadvantage in the model involves the assumption that disks of vessel-tissue systems cannot interact with each other. In other words, the neglecting of axial diffusion in the model is likely to limit the accuracy of the model radially downstream from the vessel edge. Future directions would include incorporation of axial diffusion to better understand phase effects of oxygen diffusion as a function of frequency dependent changes in convective diffusion.

5 Conclusion

The mathematical model presented allows for the determination of local changes in oxygen spatial maps as a function of the cardiac cycle and frequency dependent modulations in oxygen convection in microcirculatory networks. The results presented, in addition to validating classical microcirculatory theories of phenomena like hypoxia, hyperoxia, and vasomotion, provide a means to better understand changes in oxygen concentration at the microcirculatory level as a function of systemic hemodynamic parameters. Future directions include further numerical complications of the model in order to better understand changes in the phase of oxygen diffusion relative to frequency dependent modulations in oxygen convection.

References

[1] Vivek P. Jani, Ozlem Yalcin, Alexander T. Williams, Mark A. Popovsky, and Pedro Cabrales. Rat red blood cell storage lesions in various additive solutions. *Clinical Hemorheology and Microcirculation*, pages 1–13, 2017.

[2] Iskra Stefanova, Thomas Stephan, Sandra Becker-Bense, Thomas Dera, Thomas Brandt, and Marianne Dieterich. Age-related changes of blood-oxygen-level–dependent signal dynamics during optokinetic stimulation. *Neurobiology of Aging*, 34(10):2277–2286, oct 2017.

[3] Pedro Cabrales. Effects of erythrocyte flexibility on microvascular perfusion and oxygenation during acute anemia. *American Journal of Physiology - Heart and Circulatory Physiology*, 293(2):H1206 LP – H1215, aug 2007.

[4] V P Jani, S Mailo, A Athar, A Lucas, A T Williams, and P Cabrales. Blood Quality Diagnostic Device Detects Storage Differences Between Donors, 2017.

[5] S A McLellan and T S Walsh. Oxygen delivery and haemoglobin. *Continuing Education in Anaesthesia Critical Care & Pain*, 4(4):123–126, aug 2004.

[6] Julie-Ann Collins, Aram Rudenski, John Gibson, Luke Howard, and Ronan O'Driscoll. Relating oxygen partial pressure, saturation and content: the haemoglobin–oxygen dissociation curve. *Breathe*, 11(3):194–201, sep 2015.

[7] Roland N Pittman, Aleksander S Golub, and Helena Carvalho. Measurement of Oxygen in the Microcirculation Using Phosphorescence Quenching Microscopy BT - Oxygen Transport to Tissue XXXI. pages 157–162. Springer US, Boston, MA, 2010.

[8] M Sharan, M P Singh, and B Singh. An analytical model for oxygen transport in tissue capillaries in a hyperbaric environment with first order metabolic consumption. *Mathematical and Computer Modelling*, 22(9):99–111, 1995.

[9] Andreas Jung, Rupert Faltermeier, Ralf Rothoerl, and Alexander Brawanski. A mathematical model of cerebral circulation and oxygen supply. *Journal of Mathematical Biology*, 51(5):491–507, 2005.

[10] Timothy W Secomb. Krogh-cylinder and infinite-domain models for washout of an inert diffusible solute from tissue. *Microcirculation (New York, N.Y. : 1994)*, 22(1):91–98, jan 2015.

[11] Aleksander S Golub and Roland N Pittman. Po₂ measurements in the microcirculation using phosphorescence quenching microscopy at high magnification. *American Journal of Physiology - Heart and Circulatory Physiology*, 294(6):H2905 LP – H2916, jun 2008.

[12] Franziska Heu, Clemens Forster, Barbara Namer, Adrian Dragu, and Werner Lang. Effect of low-level laser therapy on blood flow and oxygen- hemoglobin saturation of the foot skin in healthy subjects: a pilot study. *Laser Therapy*, 22(1):21–30, jan 2013.

[13] A J Pahnvar, A Işıkhan, İ Akkaya, Y Efteli, M Engin, and E Z Engin. Estimation of oxygen saturation with laser optical imaging method, 2016.

[14] Richard A Bader, Mortimer E Bader, and Joel L Duberstein. Polycythemia vera and arterial oxygen saturation. *The American Journal of Medicine*, 34(4):435–439, oct 2017.

A Table of Parameters

Measurement	Value	Units
Diameter (d)	40	μm
Length (L)	100	μm
Diffusivity (D)	1.80E-05	cm^2/s
O2 in	60	mmHg
O2 out	55	mmHg
Heart rate (HR)	450	BPM
Partition Coefficient (ϕ)	0.50	-
Henry's Law Constant (α)	0.4466	mol/(m^3*mmHg)

Figure A.1: Table of Relevant Parameters

B Matlab Code

Contents

Numerical Sol'n of Steady State Model

```
%%%%%%%% SOLN FOR VESSEL

O2in = 60; %mmHg
O2out = 55; %mmHg
L = 100; %μm
conc = zeros(1,100);
for z = 1:100; %10000 to see the decay non linear
conc(z) = O2in * (O2out / O2in)^(z / L);
end
conc(1) = 60;

%%%%%%%% SOLN FOR TISSUE
iot = .5;
x=1;
D = 1.75e-5;
alph = 3e-5;
r = 80;
delr = 1;
conc = zeros(1,80);
conc(1) = 60 * alph;
conc(2) = conc(1);
k=.5;

%collect data using for loop
```

```
for n = 2:79;
    conc(n+1) = (1/(1+(delr/r))*((2 + (delr/r) - ...
        (delr^2*(k^(1/3)/D))*conc(n)^(1/3))-conc(n-1)));
end

%plot the concentration along the axis
%plot(1:80,conc)
%viewing just the inside of the vessel
% conc = [conc;conc;conc;conc];
% surf(conc)
% title('Oxygen Conc. down the length of the vessel')
% xlabel('z (distance from start of the vessel μm)')
% zlabel('[O_2]')

%viewing everything outside the vessel
mesh(O2concProfile(conc))
xlabel('distance from vessel')
ylabel('length vessel')
zlabel('[O_2]')

title('[O_2] profile in surrounding tissue')
```

O2 Conc Profile Function

```
[out] = @O2concProfile(cin)
r = (21:1:100);
x = (1:1:100);
out = zeros(length(x),length(r));
phi = 0.5;
D = 1.75e-5; %cm^2/s
R = 20; %μm
v = 20; %mm/s
L = 100; %μm
alph = 3e-5; %conversion factor
O2in = 60 * alph;
O2out = 55 * alph;
k_leak = (v/L)*log(O2in/O2out);
k_cons = 0.5*k_leak;
for i = 1:length(x)
    for j = 1:length(r)
        out(i,j) = phi*cin(i)*(sqrt(-(k_cons/D))*R)/(sqrt(-(k_cons/D))*r(j));
    end
end
```

Numerical Sol'n of Non - Steady State Model

```
%%Constant Definition
v = 20e-3; % m/s
d = 40e-6; % m
R = d/2; % radius
L = 100e-6; % m
D = 18e-10; % m^2/s
o2in = 60*364/815; % mol/m^3
o2out = 55*364/815; % mol/m^3
HR = 450; % bpm
Phi = 0.5; % partition coefficient
```

Axial Problem

```
% Boundary Conditions
fax = @(t) sin(pi.*HR.*t./30)+o2in;
gax = @(t) sin(pi.*HR.*t./30)+o2out;

% Solution
cin = @(z,t) (fax(t - (z./v)).*((gax(t)./fax(t - (L./v)))).^(z./L)).*(815/364);
step = 7.5/1000;
```

```
[Z,T] = meshgrid(0:(L/100):L,0:step:5);
CIN = cin(Z,T);
% surf(Z,T,CIN)
```

Radial Problem

```
% For this iteration, we are just testing, so I will assume z = 0. To
% generate the image plot in 4D, I will do it for all z

% Miscellaneous Necessary parameters
% Use k at t =0 to approximate k
sc = 0.1; %scaling factor for variation in k
k = log(gax(0)/fax(-L/v))*(v/L)*Phi * sc;
Rdom = linspace(R,5*R,1000); % Domain of the problem from R to 5R

% Boundary Conditions
hout = @(z,t) Phi*cin(z,t);

% Initial Condition
fout = @(r,z) Phi.*cin(z,0).*10.^((R-r)./(4*R));
fbar = @(r,z) fout(r,z).*b(r,z,0);

% First 100 Roots of the Bessel Function of the first kind
alpha = besselzero(0,100,1);

% Eigenvalues:
lambda = D.*((alpha./R).^2)-k;
mlam = max(lambda);
lambda = lambda./max(lambda);

% Eigenfunctions
eigsoln = myeig(k,D,lambda,Rdom);
rint = linspace(R,1,10000);
eigint = myeig(k,D,lambda,rint);

% To define nonhomogeneous term, we need to take time derivative of cin
shift = sqrt(-k/D);
syms t
hout_sym = sym(hout);
dhout = diff(hout_sym,t);
dhout = matlabFunction(dhout);
clear t;
b = @ (r,z,t) (besselk(0,shift*r)./besselk(0,shift*R)).*hout(z,t);
Q = @(r,z,t) (besselk(0,shift*r)./besselk(0,shift*R)).*dhout(t,z);


% Calculating Integral for coefficients bn(t) (known as beta_n in scratch
% paper) - Simplified by separating out cin(z,t) from the equation
beta = get_beta(k,lambda,R,D,eigint,rint);

% To determine the solution for all space and all time
% Notes: r = Rdom for the input
Zdom = linspace(0,L,10);
Rdom = linspace(R,50*R,10);
tin = 0:step:5;
final_out_smallk = ones(length(Zdom),length(Rdom),length(tin));
scaling = 0.009944751089163;
count = 0;

for ii = 1:length(Zdom)
    dummy_z = Zdom(ii);
    count = count+1;
    disp(count)
    for jj = 1:length(Rdom)
        dummy_r = Rdom(jj);
        an_init = an_initial(Phi,cin,R,eigint,rint,lambda,dummy_z,k,D);
        an_all = a_n(dummy_z,tin,lambda,beta,dhout,an_init);
        tvec_cout = ctissue(k,lambda,D,an_all,R,hout,Phi,cin,dummy_r,dummy_z,tin);
        tvec_cout = tvec_cout.*scaling;
        final_out_smallk(ii,jj,:) = tvec_cout;
```

```
    end
end
```

Ctissue function

```
out = @ctissue(k,lambda,D,an_all,R,hout,Phi,cin,r,z,tin)

shift1 = sqrt(-k/D);
b = @ (r,z,t) (besselk(0,shift1*r)./besselk(0,shift1*R)).*hout(z,t);

sum_vec = zeros(length(tin),1);

for ii = 1:length(lambda)
    shift = sqrt((k+lambda(ii))/D);
    an = an_all(:,ii);
    phinr = besselj(0,shift*r);
    dummy = phinr.*an;
    dummy = dummy.'+ b(r,z,tin);
    sum_vec = sum_vec + dummy.';
end

out = sum_vec';
```

myeig Function

```
A = @myeig(k,D,lambda,r)


    eigmat = zeros(length(r),length(lambda));

    for ii = 1:length(lambda)
        val = (k + lambda(ii))/D;
        val = abs(val);
        val = sqrt(val);
        val = val.*r;
        val = besselj(0,val);
        eigmat(:,ii) = val;

    end


A = eigmat;
```

besselzero Function

```
x=@besselzero(n,k,kind)

k3=3*k;

x=zeros(k3,1);

for j=1:k3

    % Initial guess of zeros
    x0=1+sqrt(2)+(j-1)*pi+n+n^0.4;

    % Do Halley's method
    x(j)=findzero(n,x0,kind);

    if x(j)==inf
        error('Bad guess.');
    end

end

x=sort(x);
dx=[1;abs(diff(x))];
```

```
x=x(dx>1e-8);

x=x(1:k);
```

findzero Function

```
x=@findzero(n,x0,kind)

n1=n+1;     n2=n*n;

% Tolerance
tol=1e-12;

% Maximum number of times to iterate
MAXIT=100;

% Initial error
err=1;

iter=0;

while abs(err)>tol & iter<MAXIT

    switch kind
        case 1
            a=besselj(n,x0);
            b=besselj(n1,x0);
        case 2
            a=bessely(n,x0);
            b=bessely(n1,x0);
    end

    x02=x0*x0;

    err=2*a*x0*(n*a-b*x0)/(2*b*b*x02-a*b*x0*(4*n+1)+(n*n1+x02)*a*a);

    x=x0-err;
    x0=x;
    iter=iter+1;

end

if iter>MAXIT-1
    warning('Failed to converge to within tolerance. ',...
            'Try a different initial guess');
    x=inf;
end
```

an_initial Function

```
out = @an_initial(Phi,cin,R,eigint,rint, lambda, z,k,D)

dem = zeros(length(lambda),1);

for jj = 1:length(lambda)
    eigdem = eigint(:,jj);
    eigdem = eigdem.*eigdem;
    predem = eigdem.*rint.';
    predem = trapz(rint,predem);
    dem(jj) = predem;
end

shift = sqrt(-k/D);
hout = @(z,t) Phi*cin(z,t);
fout = @(r,z) Phi.*cin(z,0).*10.^((R-r)./(4*R));
b = @ (r,z,t) (besselk(0,shift*r)./besselk(0,shift*R)).*hout(z,t);
fbar = @(r,z) fout(r,z).*b(r,z,0);
fint = fbar(rint,z);
fint = fint.';
```

```
num = zeros(length(lambda),1);

for ii = 1:length(lambda)
    eig = eigint(:,ii);
    prenum = eig.*fint;
    prenum = prenum.*rint.';
    prenum = trapz(rint,prenum);
    num(ii) = prenum;
end

ano = num./dem;

out = ano;
```

a_n Function

```
out = @a_n(z,tin,lambda,beta,dhout,an_init)

num = length(lambda);
step = tin(2)-tin(1);

out = zeros(length(tin),num);

for ii = 1:num
    vec = zeros(size(tin));
    vec(1) = an_init(ii);
    for jj = 1:(length(tin)-1)
       vec(jj+1) = (beta(ii)*dhout(z,tin(jj))  - lambda(ii)*vec(jj))*step + vec(jj);
    end
    out(:,ii) = vec.';
end
```